Herschel: the first science highlights

LETTER TO THE EDITOR

Herschel-SPIRE FTS spectroscopy of the carbon-rich objects AFGL 2688, AFGL 618, and NGC 7027[⋆,⋆⋆]

R. Wesson[1], J. Cernicharo[2], M. J. Barlow[1], M. Matsuura[1,3], L. Decin[4,5], M. A. T. Groenewegen[6], E. T. Polehampton[7,8], M. Agundez[9], M. Cohen[10], F. Daniel[2], K. M. Exter[4], W. K. Gear[11], H. L. Gomez[11], P. C. Hargrave[11], P. Imhof[12], R. J. Ivison[13], S. J. Leeks[7], T. L. Lim[7], G. Olofsson[14], G. Savini[1], B. Sibthorpe[13], B. M. Swinyard[7], T. Ueta[15], D. K. Witherick[1], and J. A. Yates[1]

(Affiliations are available in the online edition)

ABSTRACT

We present far-infrared and submillimetre spectra of three carbon-rich evolved objects, AFGL 2688, AFGL 618 and NGC 7027. The spectra were obtained with the SPIRE Fourier-transform spectrometer on board the *Herschel* Space Observatory, and cover wavelengths from 195–670 μm, a region of the electromagnetic spectrum hitherto difficult to study in detail. The far infrared spectra of these objects are rich and complex, and we measure over 150 lines in each object. Lines due to 18 different species are detected. We determine physical conditions from observations of the rotational lines of several molecules, and present initial large velocity gradient models for AFGL 618. We detect water in AFGL 2688 for the first time, and confirm its presence in AFGL 618 in both ortho and para forms. In addition, we report the detection of the $J = 1$–0 line of CH$^+$ in NGC 7027.

Key words. astrochemistry – line: identification – circumstellar matter – stars: evolution – stars: general – infrared: stars

1. Introduction

Low- to intermediate-mass stars (<8 $M_\odot$) shed much of their mass during the final stages of their evolution, in the form of a slow molecular wind. The mass loss causes the star to leave the asymptotic giant branch (AGB), moving to the left in the Hertzsprung-Russell diagram. The star becomes hotter, warming and eventually ionising its previously ejected outer layers, which become visible as a planetary nebula (PN). The ejecta from such stars are a major contributor to galactic chemical evolution (e.g. Matsuura et al. 2009).

The evolution from the AGB to the PN stage is rapid, and relatively few objects in this intermediate stage are known (326 are listed by Szczerba et al. 2007, compared to around 3000 known or suspected PNe Frew & Parker 2010). AFGL 618 and AFGL 2688 (the Egg Nebula) are two of the best-known objects in this transition stage. AFGL 2688 is illuminated by a central star with spectral type F5, and Hubble Space Telescope images reveal a large number of round arcs crossed by "searchlight beams" (Sahai et al. 1998). Proper motion measurements give a distance of 420 pc and a dynamical age for the ejected material of 350 years (Ueta et al. 2006). AFGL 618 entered the protoplanetary nebula (PPN) phase 100–200 years ago (Kwok & Bignell 1984; Bujarrabal et al. 1988), and is more evolved than AFGL 2688. It contains a B0 central star surrounded by a compact H II region (Wynn-Williams 1977; Kwok & Bignell 1984). The variability of free-free emission from this object

over the last 30 years implies rapid evolution (Kwok & Feldman 1981; Sánchez Contreras et al. 2002). NGC 7027 is a very young planetary nebula (Masson 1989). It has been extensively studied due to its high surface brightness at all wavelengths, and observations with the ISO revealed a far-infrared spectrum rich in atomic and molecular lines (Liu et al. 1996). Its ionised inner regions are surrounded by and partly obscured by a PDR and massive molecular envelope.

Previous far infrared and sub-mm observations of these evolving post-AGB objects, although limited in their spatial resolution and spectral coverage, have revealed rich spectra containing numerous molecular and dust features (e.g. Cox et al. 1996; Liu et al. 1996; Herpin et al. 2000; Pardo et al. 2004, 2005; Pardo & Cernicharo 2007; Pardo et al. 2007). The *Herschel* Space Observatory (Pilbratt et al. 2010) now significantly extends our observational capabilities. The SPIRE spectrometer covers wavelengths from 195–670 μm, a region of the electromagnetic spectrum hitherto largely unexplored. The SPIRE instrument, its in-orbit performance, and its scientific capabilities are described by Griffin et al. (2010), and the SPIRE astronomical calibration methods and accuracy are outlined by Swinyard et al. (2010). Here we present observations of AFGL 2688, AFGL 618 and NGC 7027 using the SPIRE spectrometer.

2. Observations

Observations of AFGL 2688, AFGL 618 and NGC 7027 were obtained using the SPIRE Fourier-transform spectrometer, which covers short (SSW, 194–313 μm) and long (SLW, 303–671 μm) wavelength bands simultaneously. We combine data taken during the satellite's performance verification phase with data taken during the science demonstration phase for the

---
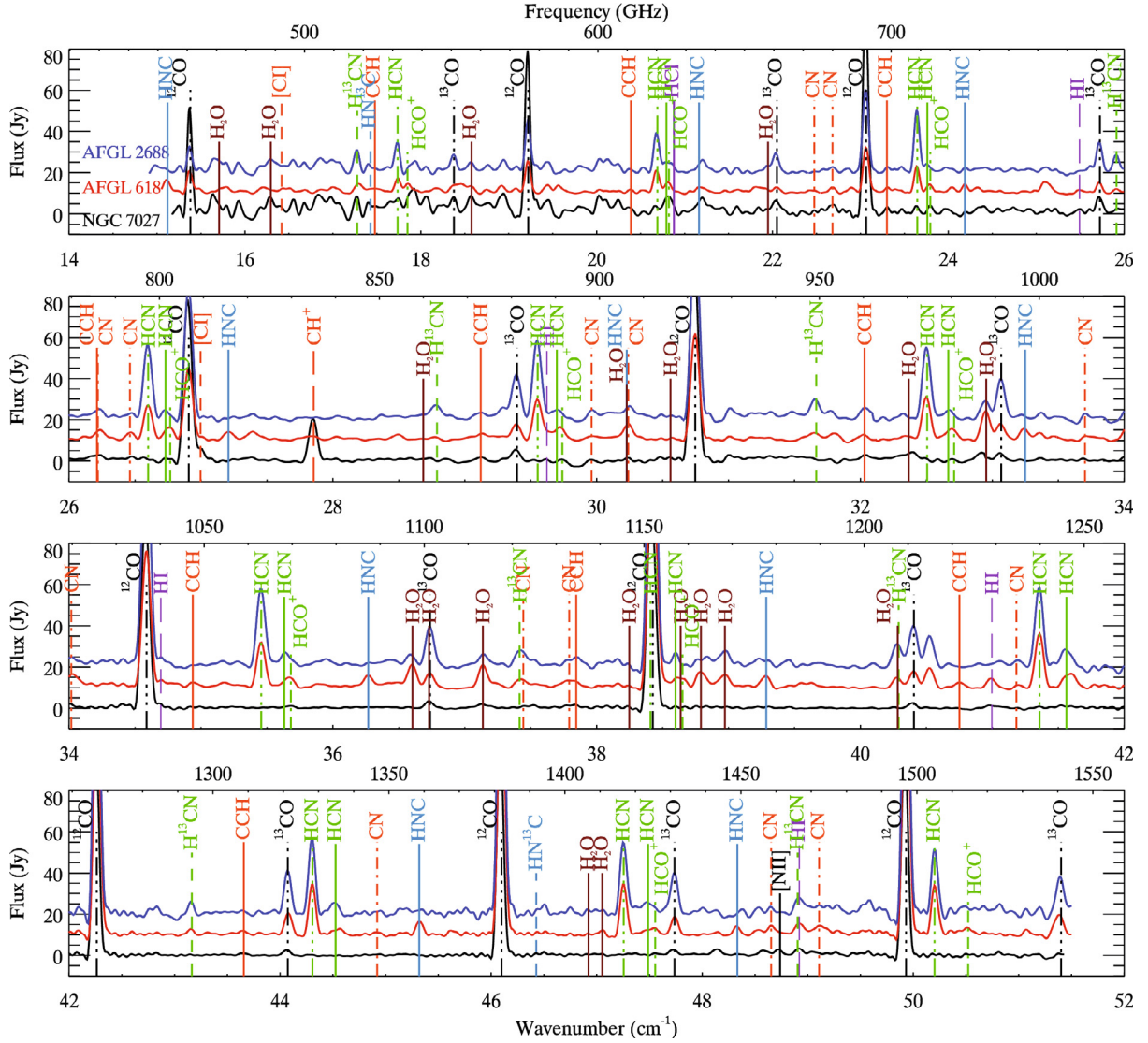
Fig. 1. Continuum-subtracted SPIRE FTS spectra of NGC 7027 (black), AFGL 618 (red) and AFGL 2688 (blue). For clarity, the spectrum of NGC 7027 is multiplied by a factor of two, the spectrum of AFGL 618 is offset by 10 Jy, and the spectrum of AFGL 2688 is offset by 20 Jy.

Mass-loss of Evolved StarS (MESS[1]) guaranteed time program (Groenewegen et al., in prep.). We reduced the spectra with the *Herschel* interactive processing environment software (HIPE), using the standard point-source pipeline described by Swinyard et al. (2010). A dark-sky observation taken close to the time of the object observations was subtracted to correct for telescope and sky emission, and the spectra were flux-calibrated using observations of the asteroid Vesta. We combined three observations of AFGL 618, five of AFGL 2688 and seven of NGC 7027 to obtain our final spectra. The total on-source exposure times were 11 988s (AFGL 618), 4 928 s (AFGL 2688) and 11 188 s (NGC 7027).

The FTS produces spectra in which the line profiles are sinc functions; to eliminate the negative side-lobes this produces, we apodized the interferograms using the extended Norton-Beer function 1.5 (Naylor & Tahic 2007). This results in line profiles which are close to Gaussian, with a full width at half-maximum ($FWHM$) of 0.070 cm^{-1} (2.1 GHz). We then measured line intensities using the ELF Gaussian fitting routine in DIPSO (Howarth et al. 2004). We detected 203 lines in AFGL 2688,

214 in AFGL 618 and 164 in NGC 7027. We present plots of the continuum-subtracted spectra in Fig. 1.

3. Line measurements

Most strong lines in our spectra are readily identified, although a number of lines remain unidentified at this stage. Table 1, available online, contains measured line intensities and identifications for each object spectrum; Tables 2–4 list the strongest unidentified lines. The quoted uncertainties are from the line fitting only; the absolute uncertainties on the flux calibration are estimated to be 10-20% in the SSW band and ∼30% in the SLW band.

CO: All three spectra are dominated by the rotational lines of ^{12}CO. We plot rotational diagrams using the method described by Justtanont et al. (2000). Figure 2 shows plots for ^{12}CO and ^{13}CO for our targets, using all the observed lines, from $J = 4$–3 to $J = 13$–12 for ^{12}CO, and $J = 5$–4 to $J = 14$–13 for ^{13}CO. The CO $J = 10$–9 line at 38.426 cm^{-1} is blended with HCN $J = 13$–12 at 38.408 cm^{-1}, and we estimate the relative contribution of the two species by linearly interpolating between the fluxes of the two neighbouring lines. The sum of these estimated fluxes is within 3 per cent of the measured flux of the blend.
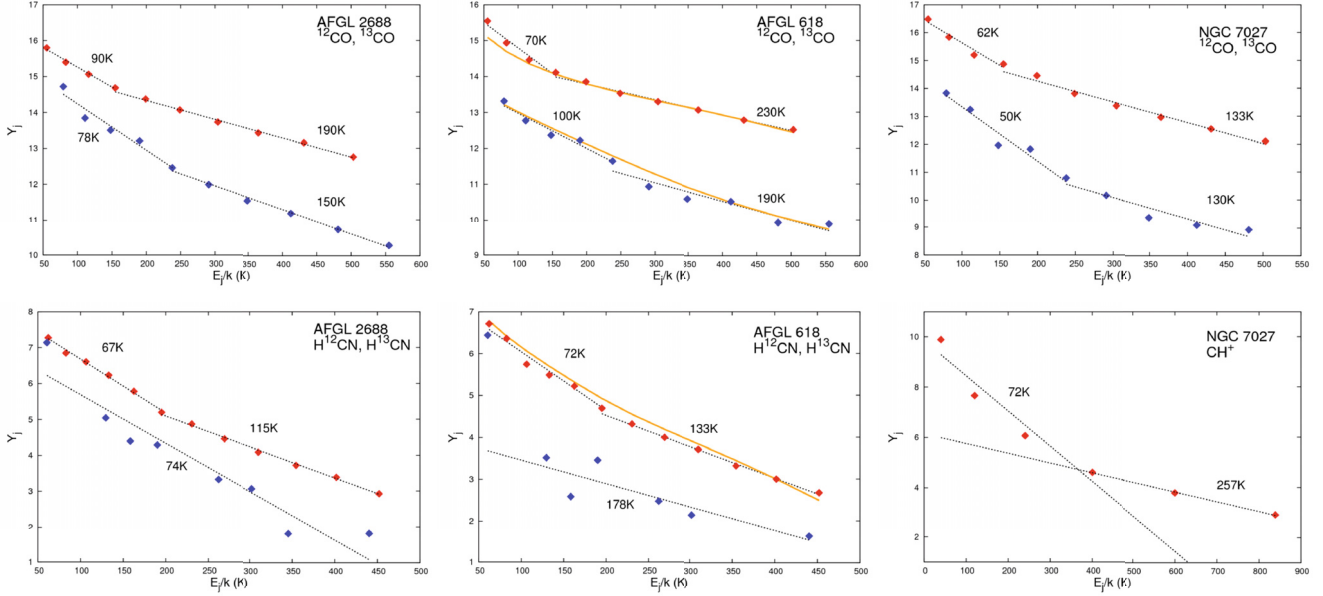
Fig. 2. Rotation diagrams based on fluxes measured in our SPIRE FTS spectra. $Y_j = ln(4\pi F_{ji}/A_{ji}h\nu_{ji}g_j)$, where F_{ji} is the line flux in Wm^{-2}, A_{ji} is the Einstein coefficient for spontaneous emission, ν_{ji} is the frequency of the transition and g_j is the statistical weight of the upper level j. The object and species are labelled in each panel. Red points indicate species containing ^{12}C, and blue points indicate ^{13}C. The temperatures derived from the slopes of the diagrams are indicated. The CO, H^{12}CN and CH$^+$ data points clearly steepen at lower E_j and we fit these data with two components. H^{13}CN data points are fitted with a single line. The orange lines on the diagrams for AFGL 618 represent the predictions of our LVG models, described in Sect. 4.

We derive rotational temperatures by fitting a line to the observed points, with the slope of the line being equal to $1/T_{rot}$. The data clearly cannot be fitted by a single temperature, and so for ^{12}CO we fit the data for $J_{up} \leq 7$ and $J_{up} \geq 8$ separately, while for ^{13}CO we fit the data for $J_{up} \leq 9$ and $J_{up} \geq 10$ separately. The temperatures we derive lie between 60 and 230 K, and are shown on the plots in Fig. 2. The uncertainties on the rotational temperatures are typically 10–20 K.

Justtanont et al. (2000) find considerably higher temperatures following this approach for lines up to $J = 37$–36 observed in ISO-LWS spectra; plotting the new *Herschel* data together with the ISO data clearly shows that the CO lines cannot be described by a uniform rotational temperature, with the higher-J lines requiring higher temperatures. This indicates that the low-J lines are tracing the extended AGB envelope, while the higher-J lines are tracing hotter gas from the inner layers of the outflow. Models produced by Herpin & Cernicharo (2000) and Herpin et al. (2002) use several spatial components at different temperatures to reproduce the observed emission from these objects.

HCN: We also plot rotation diagrams for H^{12}CN and H^{13}CN in AFGL 2688 and AFGL 618, where these species are well detected (Fig. 2). We derive rotation temperatures from fits to the observed points, using the interpolated flux described above for the $J = 13$–12 transition of H^{12}CN, which is blended with the ^{12}CO $J = 10$–9 line. The temperatures we derive are comparable to those derived from the ^{13}CO lines, suggesting that these species trace similar regions of the circumstellar environments.

Rotational lines of vibrationally-excited HCN lines can be prominent in the AGB phase of carbon-rich stars (Cernicharo et al. 1996), and we detect them in AFGL 2688 and AFGL 618. At the resolution of the SPIRE spectrometer, the $l = -1$ component of the $\nu_2 = 1$ level is blended with the ground state HCN lines, while the $l = +1$ component lines lie within one resolution element of those of HCO$^+$; ionised molecular species have very low abundances in AFGL 2688 and so we attribute lines at the frequencies of HCN $\nu_2 = 1$ to this species alone. In AFGL 618, if the blend is not resolved we attribute the lines to both HCO$^+$ and HCN $\nu_2 = 1$.

H$_2$O: Herpin & Cernicharo (2000) detected lines due to ortho-H$_2$O in AFGL 618 in ISO spectra. We now also detect para-H$_2$O in this object, and we also detect water lines from AFGL 2688 for the first time. We also detect seven low-lying water lines from NGC 7027. The origin of oxygen-bearing molecules in carbon-rich objects is not well understood, given the expectation that all oxygen molecules will be locked up in CO with none left over to form oxygen-bearing molecules. They may trace much older regions of the outflow from the star, from a time when its surface composition was oxygen-rich. Cernicharo et al. (2004) showed that photodissociation of CO by the stellar UV field followed by reactions with H$_2$ can account for the observed abundance of H$_2$O in AFGL 618; AFGL 2688's much cooler central star makes a similar origin unlikely. Alternative production mechanisms include the vaporization of icy bodies (Melnick et al. 2001), Fischer-Tropsch catalysis on grain surfaces (Willacy 2004) and radiative association between atomic oxygen and molecular hydrogen during the AGB phase (Agúndez & Cernicharo 2006). Another possibility that should be explored is how deep interstellar UV photons can penetrate into the envelope. The circumstellar envelope of AFGL 2688 is formed by a series of concentric shells rather than a continuous envelope (Sahai et al. 1998), and if interstellar UV photons can reach its warm inner regions, then a very rich chemistry could be triggered by the photodissociation of CO and other species. In the case of NGC 7027, water lines were tentatively identified in ISO-LWS spectra by Cernicharo et al. (1997) and Liu et al. (1997). Yan et al. (1999) and Agúndez et al. (2010) showed that H$_2$O could form in NGC 7027's warm, dense PDR through reactions involving vibrationally-excited H$_2$.

CH$^+$: Lines due to ionised species are absent in the spectrum of AFGL 2688, weak in AFGL 618 and strong in NGC 7027. The CH$^+$ line at 27.855 cm^{-1} is very bright in NGC 7027, and

we combine our observation with LWS observations of higher-J CH^+ lines from Cernicharo et al. (1997) to produce the rotation diagram in Fig. 2. The data cannot be fitted by a single temperature, and we derive $T_{rot} = 72 \pm 12$ K for $E_j < 400$ K, and $T_{rot} = 257 \pm 8$ K for $E_j > 400$ K. These temperatures are far lower than the ~4300 K activation energy of the reaction $C^+ + H_2 \rightarrow CH^+ + H$. However, under the simplifying assumptions of low optical depth and LTE, the derived rotational temperature is a lower limit to the kinetic temperature. Agúndez et al. (2010) find that CH^+ in NGC 7027 is formed both via this reaction in warm gas ($T_k > 400$–500 K) and via the reaction of vibrationally excited H_2 with C^+.

4. LVG models for AFGL 618

To further investigate the nature of AFGL 618, we constructed a large velocity gradient (LVG) model, based initially on that of Herpin & Cernicharo (2000), in which the object is modelled as a torus surrounded by a high-velocity wind (HVW) region, with the ejecta from the earlier AGB phase further out. Material in the torus is at temperatures from 250–1000 K; the HVW region consists mostly of 200 K material with a small amount of hotter gas at 1000 K, and the AGB remnant has a temperature of 100 K. The CO rotation temperatures derived by Justtanont et al. (2000) from ISO data, and in this paper from *Herschel* data, are consistent with the model temperatures, with ISO sampling the warmer material and *Herschel* being sensitive to the cooler material further from the central star. We used the model to predict ^{12}CO, ^{13}CO, $H^{12}CN$ and $H^{13}CN$ fluxes.

Matching our observed ^{12}CO and ^{13}CO fluxes was possible with almost exactly the same model parameters for CO as given in Table 1 of Herpin & Cernicharo; the only change was to reduce the ^{13}CO column density in the AGB ejecta from 3.5×10^{17} cm^{-2} to 2.5×10^{17} cm^{-2}, reducing the total ^{13}CO column density by 7%. This is well within the estimated model uncertainties of 20–30%. A good match to the observed $H^{12}CN$ intensities required a total column density of HCN a factor of 5 lower than the value found by Herpin & Cernicharo (2000). This reflects the different regimes to which ISO and *Herschel* are sensitive, with *Herschel* providing information about much cooler regions than could be observed with ISO. The match to the $H^{13}CN$ intensities is poor; these lines are quite weak in AFGL 618 and may be blended. We plot the predictions of the model for ^{12}CO, ^{13}CO and $H^{12}CN$ on the rotation diagrams in Fig. 2.

The $^{12}C/^{13}C$ ratio is a tracer of the history of nuclear processing inside stars. ^{13}C is an intermediate product in the CNO cycle which is the main fusion reaction converting hydrogen into helium in stars with masses >1.2 $M_\odot$, and lower $^{12}C/^{13}C$ ratios result from CNO cycle material being brought to the surface. Milam et al. (2009) find that carbon-rich stars have $^{12}CO/^{13}CO$ ratios generally in the range 25–90. To match the observed CO line fluxes in AFGL 618 requires a $^{12}C/^{13}C$ ratio of 21 in our model, implying substantial ^{13}C enrichment. Pardo & Cernicharo (2007) find a $^{12}C/^{13}C$ ratio of ~15 in regions closest to the central star and ~40 in regions further out, possibly indicating a late ejection of ^{13}C-rich material from the star.

5. Conclusions

The unprecedented wavelength coverage and excellent sensitivity of the SPIRE spectrometer have allowed us to see the incredibly rich far-infrared and submm spectra of three carbon-rich evolved stars for the first time. We have detected 150–200 emission lines in the SPIRE FTS spectra of AFGL 2688, AFGL 618 and NGC 7027, and presented preliminary investigations of the physical conditions in these objects based on the new data. We find water in both ortho and para forms in all three objects, and observe strong ionised lines in the more evolved NGC 7027, including the $J = 1$–0 line of CH^+. This line, never previously detected in an astronomical source, is also detected in *Herschel* spectra of H II region PDRs (Naylor et al. 2010). LVG models of AFGL 618 are in excellent agreement with those based on earlier ISO data. These observations show that the SPIRE spectrometer on board *Herschel* can provide significant new insights into the temperatures structure and chemical content of the outflows from evolved stars.

References

Agúndez, M., & Cernicharo, J. 2006, ApJ, 650, 374
Agúndez, M., Goicoechea, J. R., Cernicharo, J., et al. 2010, ApJ, 713, 662
Bujarrabal, V., Gomez-Gonzalez, J., Bachiller, R., & Martin-Pintado, J. 1988, A&A, 204, 242
Cernicharo, J., Barlow, M. J., González-Alfonso, E., et al. 1996, A&A, 315, 201
Cernicharo, J., Liu, X.-W., González-Alfonso, E., et al. 1997, ApJ, 483, L65
Cernicharo, J. 2004, ApJ, 608, 41
Cox, P., González-Alfonso, E., Barlow, M. J., et al. 1996, A&A, 315, 265
Frew, D. J., & Parker, Q. A. 2010, PASA, 27, 129
Griffin, M. J., Abergel, A., Abreu, A., et al. 2010, A&A, 518, L3
Herpin, F., & Cernicharo, J. 2000, ApJ, 530, 129
Herpin, F., Goicoechea, J. R., Pardo, J. R., & Cernicharo, J. 2002, ApJ, 577, 961
Howarth, I. D., Murray, J., & Mills, D. 1994, Starlink User Note, No. 50.15
Justtanont, K., Barlow, M. J., Tielens A. G. G. M., et al. 2000, A&A, 360, 1117
Kwok, S., & Feldman, P. A. 1981, ApJ, 247, L67
Kwok, S., & Bignell, R. C. 1984, ApJ, 276, 544
Liu, X.-W., Barlow, M. J., Nguyen-Q-Rieu, et al. 1996, A&A, 315, 257
Liu, X.-W., Barlow, M. J., Dalgarno, A., et al. 1997, MNRAS, 290, 71
Masson, C. R. 1989, ApJ, 336, 294
Matsuura, M., Barlow, M. J., Zijlstra, A. A., et al. 2009, MNRAS, 396, 918
Melnick, G., et al. 2001, Nature, 412, 160
Milam, S. N., Woolf, N. J., & Ziurys, L. M. 2009, ApJ, 690, 837
Naylor, D. A., & Tahic, M. K. 2007, J. Opt. Soc. Am. A, 24, 3644
Naylor, D. A., Dartois, E., Habart, E., et al. 2010, A&A, 518, L117
Pardo, J. R., & Cernicharo, J. 2007, ApJ, 654, 978
Pardo, J. R., Cernicharo, J., Goicoechea, J. R., & Phillips, T. G. 2004, ApJ, 615, 495
Pardo, J. R., Cernicharo, J., & Goicoechea, J. R. 2005, ApJ, 628, 275
Pardo, J. R., Cernicharo, J., Goicoechea, J. R., Guélin, M., & Asensio Ramos, A. 2007, ApJ, 661, 250
Pilbratt, G. L., Riedinger, J. R., Passvogel, T., et al. 2010, A&A, 518, L1
Sahai, R., Trauger, J. T., Watson, A. M., et al. 1998, ApJ, 493, 301
Sánchez Contreras, C., Bujarrabal, V., Castro-Carrizo, A., Alcolea, J., & Sargent, A. 2004, ApJ, 617, 1142
Swinyard, B. M., Ade, P., Baluteau, J.-P., et al. 2010, A&A, 518, L4
Szczerba, R., Siódmiak, N., Stasińska, G., & Borkowski, J. 2007, A&A, 469, 799
Ueta, T., Murakawa, K., & Meixner, M. 2006, ApJ, 641, 1113
Willacy 2004, ApJ, 600, 87
Wynn-Williams, C. G. 1977, MNRAS, 181, 61
Yan, M., Federman, S. R., Dalgarno, A., & Bjorkman, J. E. 1999, ApJ, 515, 640

Pages 5 to 8 are available in the electronic edition of the journal at `http://www.aanda.org`

[1] Department of Physics and Astronomy, University College London, Gower Street, London WC1E 6BT, UK
e-mail: rwesson@star.ucl.ac.uk

[2] Astrophysics Dept, CAB (INTA-CSIC), Crta Ajalvir km4, 28805 Torrejon de Ardoz, Madrid, Spain

[3] Mullard Space Science Laboratory, University College London, Holmbury St. Mary, Dorking, Surrey RH5 6NT, UK

[4] Instituut voor Sterrenkunde, Katholieke Universiteit Leuven, Celestijnenlaan 200 D, 3001 Leuven, Belgium

[5] Universiteit van Amsterdam, Sterrenkundig Instituut "Anton Pannekoek", Science Park 904, 1098 XH Amsterdam, The Netherlands

[6] Royal Observatory of Belgium, Ringlaan 3, 1180 Brussels, Belgium

[7] Space Science and Technology Department, Rutherford Appleton Laboratory, Oxfordshire, OX11 0QX, UK

[8] Institute for Space Imaging Science, University of Lethbridge, 4401 University Drive, Lethbridge, Alberta, T1K 3M4, Canada

[9] LUTH, Observatoire de Paris-Meudon, 5 Place Jules Janssen, 92190 Meudon, France

[10] Radio Astronomy Laboratory, University of California at Berkeley, CA 94720, USA

[11] School of Physics and Astronomy, Cardiff University, The Parade, Cardiff, Wales CF24 3AA, UK

[12] Blue Sky Spectroscopy, 9/740 4 Ave S, Lethbridge, Alberta T1J 0N9, Canada

[13] UK Astronomy Technology Centre, Royal Observatory Edinburgh, Blackford Hill, Edinburgh EH9 3HJ, UK

[14] Dept of Astronomy, Stockholm University, AlbaNova University Center, Roslagstulsbacken 21, 10691 Stockholm, Sweden

[15] Dept. of Physics and Astronomy, University of Denver, Mail Stop 6900, Denver, CO 80208, USA

Table 1. Line intensities and identifications in each spectrum. Rows beginning with a "+" indicate that the line is blended with that on the row above. The quantum numbers given in the "transition" column are J except where stated. H$_2$O transitions are given in the format $J'_{k'_a k'_c}$-$J_{k_a k_c}$.

$\bar{v}_0$ (cm^{-1})	λ_0 (μm)	Species	Transition	AFGL 2688 $\bar{v}_{obs}$ (cm^{-1})	F (×10^{-18} Wm^{-2})	AFGL 618 $\bar{v}_{obs}$ (cm^{-1})	F (×10^{-18} Wm^{-2})	NGC 7027 $\bar{v}_{obs}$ (cm^{-1})	F (×10^{-18} Wm^{-2})
15.119	661.40	HNC	5-4			15.111	205.8 ± 6.3		
15.239	656.23	^{12}CO	$v = 1$;4–3	15.248	63.0 ± 8.1				
15.379	650.25	^{12}CO	4–3	15.372	281.4 ± 8.7	15.369	217.8 ± 12.9	15.371	556.5 ± 6.0
15.707	636.65	p-H$_2$O	6_{42}-5_{51}			15.705	20.1 ± 18.3		
16.294	613.71	p-H$_2$O	6_{24}-7_{17}			16.275	56.4 ± 13.8	16.282	129.9 ± 21.9
16.417	609.14	[C I]	1–0					16.397	97.2 ± 21.6
17.278	578.78	H^{13}CN	6–5	17.273	256.8 ± 2.7	17.293	127.5 ± 9.0	17.259	126.3 ± 28.5
17.428	573.80	HN^{13}C	6–5	17.411	91.5 ± 8.7			17.420	60.0 ± 13.8
17.478	572.16	CCH	$N = 6$–5			17.472	165.3 ± 11.7		
17.736	563.82	HCN	6-5	17.733	325.8 ± 6.6	17.742	185.7 ± 4.2	17.748	31.8 ± 11.4
17.848	560.30	HCO$^+$	6–5			17.864	126.3 ± 3.6		
18.377	544.16	^{13}CO	5–4	18.375	243.6 ± 7.8	18.364	59.7 ± 9.0	18.377	100.5 ± 3.9
18.577	538.29	o-H$_2$O	1_{10}-1_{01}	18.571	164.4 ± 3.9	18.583	68.1 ± 4.5	18.574	154.5 ± 14.7
19.222	520.23	^{12}CO	5–4	19.222	568.2 ± 4.2	19.223	358.2 ± 1.5	19.219	882.9 ± 4.8
20.390	490.45	CCH	$N = 7$–6	20.384	39.6 ± 2.4	20.390	40.8 ± 5.1	20.374	42.3 ± 4.8
20.691	483.30	HCN	7–6	20.687	456.9 ± 3.3	20.687	279.9 ± 6.6	20.674	43.5 ± 2.7
20.793	480.93	HCN	$v_2 = 1$; 7–6f	20.787	111.6 ± 3.3	20.818	150.6 ± 6.9	20.818	157.8 ± 3.3
20.821	480.28	HCO$^+$	7–6						
20.878	478.96	HCl	1–0	20.859	100.5 ± 3.3				
21.165	472.48	HNC	7–6			21.176	89.4 ± 4.5		
21.949	455.61	p-H$_2$O	$v_2 = 1$; 1_{10}–1_{01}	21.946	70.5 ± 7.8				
22.051	453.50	^{13}CO	6–5	22.044	249.3 ± 5.1	22.054	85.5 ± 3.0	22.044	136.8 ± 4.8
22.483	444.79	CN	$N = 6$–5;$v=1$	22.489	11.7 ± 2.7				
22.683	440.86	CN	$N = 6$–5;$v=0$	22.681	73.5 ± 5.7				
22.855	437.54	^{12}CO	$v = 1$; 6–5	22.849	50.1 ± 3.3	22.872	45.6 ± 38.1		
23.065	433.56	^{12}CO	6–5	23.060	1002.0 ± 3.6	23.064	547.8 ± 4.8	23.058	1144.0 ± 5.1
23.303	429.13	CCH	$N = 8$–7	23.309	58.5 ± 3.9	23.309	76.2 ± 10.5	23.306	33.9 ± 3.6
23.646	422.91	HCN	8–7	23.643	693.9 ± 4.5	23.643	293.4 ± 5.1	23.636	40.8 ± 3.6
23.762	420.84	HCN	$v_2 = 1$; 8–7f	23.761	101.4 ± 3.6	23.789	118.2 ± 6.0	23.795	40.8 ± 4.2
23.795	420.26	HCO$^+$	8–7						
24.187	413.45	HNC	8–7	24.195	30.6 ± 9.3	24.191	110.7 ± 1.8		
25.085	398.64	o-H$_2$O	2_{11}–2_{02}			25.113	228.3 ± 4.5		
25.492	392.28	H I	H20α			25.507	50.1 ± 3.9	25.493	6.6 ± 3.3
25.724	388.74	^{13}CO	7–6	25.720	380.1 ± 7.5	25.719	121.8 ± 3.0	25.720	81.6 ± 4.5
25.912	385.92	H^{13}CN	9–8	25.914	235.2 ± 6.9	25.915	51.0 ± 1.5		
26.171	382.10	CN	$N = 7$–6; $v = 1$					26.167	28.5 ± 4.2
26.226	381.30	CCH	$N = 9$–8	26.225	148.2 ± 6.9	26.233	147.0 ± 3.0	26.230	42.9 ± 5.1
26.470	377.78	CN	$N = 7$–6; $v = 0$	26.468	56.4 ± 20.1				
26.600	375.95	HCN	9–8	26.596	855.0 ± 9.6	26.599	406.2 ± 6.3		
26.731	374.10	HCN	$v_2 = 1$; 9–8f	26.732	98.4 ± 8.7	26.756	166.2 ± 6.6		
26.767	373.59	HCO$^+$	9–8						
26.907	371.65	^{12}CO	7–6	26.905	1465.0 ± 9.3	26.907	825.9 ± 6.3	26.900	1768.0 ± 13.8
26.997	370.41	[C I]	2–1					26.997	113.4 ± 11.1
27.208	367.54	HNC	9–8			27.211	113.7 ± 2.1		
27.855	359.00	CH$^+$	1–0			27.847	65.1 ± 3.0	27.851	466.5 ± 4.5
28.685	348.61	o-H$_2$O	$v_2 = 1$; 2_{11}–2_{02}	28.677	60.9 ± 2.1	28.672	32.7 ± 8.4		
28.789	347.36	H^{13}CN	10–9	28.781	207.3 ± 2.7	28.775	33.9 ± 7.2		
29.121	343.39	CCH	$N = 10$–9	29.129	146.1 ± 7.8	29.139	91.8 ± 8.7	29.119	57.6 ± 10.2
29.396	340.18	^{13}CO	8–7	29.391	543.9 ± 5.4	29.389	202.8 ± 8.7	29.386	136.8 ± 12.6
29.553	338.38	HCN	10–9	29.550	916.8 ± 5.7	29.556	524.1 ± 9.3		
29.622	337.59	H I	H19α					29.614	10.2 ± 6.0
29.698	336.72	HCN	$v_2 = 1$; 10–9f	29.695	172.8 ± 6.9	29.715	189.6 ± 8.1	29.735	7.8 ± 5.7
29.739	336.26	HCO$^+$	10–9						
29.970	333.67	CN	$N = 8$–7;$v = 1$	29.974	117.3 ± 13.2				
30.228	330.82	p-H$_2$O	9_{28}-8_{35}	30.244	167.7 ± 13.5				
+30.229	330.81	HNC	10–9						
+30.241	330.68	CN	$N = 8$–7; $v = 0$						
30.468	328.21	^{12}CO	$v = 1$; 8–7			30.472	21.6 ± 8.4		
30.560	327.22	p-H$_2$O	4_{22}-3_{31}			30.573	26.4 ± 8.7		
30.748	325.23	^{12}CO	8–7	30.748	2073.0 ± 16.5	30.748	1229.0 ± 10.2	30.740	2249.0 ± 11.7
31.665	315.80	H^{13}CN	11–10	31.653	297.3 ± 24.0	31.651	129.3 ± 19.5		
32.030	312.21	CCH	$N = 11$–10			32.023	69.9 ± 8.1		
32.366	308.96	p-H$_2$O	5_{24}-4_{31}			32.368	81.0 ± 3.6		
32.505	307.64	HCN	11–10	32.501	818.7 ± 6.3	32.501	554.1 ± 3.6		
32.665	306.13	HCN	$v_2 = 1$; 11–10f	32.665	150.3 ± 7.8	32.703	129.3 ± 10.5	32.702	38.7 ± 2.7
32.711	305.71	HCO$^+$	11–10						
32.954	303.46	p-H$_2$O	2_{02}−1_{11}	32.946	236.4 ± 7.2	32.952	340.2 ± 3.6	32.943	44.1 ± 3.3
33.067	302.41	^{13}CO	9–8	33.066	457.2 ± 7.5	33.066	202.5 ± 3.9	33.060	87.0 ± 3.3
33.249	300.76	HNC	11–10			33.244	142.2 ± 3.6		

Table 1. continued.

$\bar{v}_0$ (cm⁻¹)	λ_0 (μm)	Species	Transition	AFGL 2688		AFGL 618		NGC 7027	
				$\bar{v}_{\rm obs}$ (cm⁻¹)	F(×10⁻¹⁸ Wm⁻²)	$\bar{v}_{obs}$ (cm⁻¹)	F(×10⁻¹⁸ Wm⁻²)	$\bar{v}_{\rm obs}$ (cm⁻¹)	F(×10⁻¹⁸ Wm⁻²)
33.711	296.64	CN	$N = 9\text{–}8; v = 1$			33.708	33.6± 32.4		
34.026	293.90	CN	$N = 9\text{–}8; v = 0$	34.030	124.8± 13.8	34.039	230.7 ± 14.4		
34.588	289.12	^{12}CO	9-8	34.585	2711.0 ± 17.4	34.586	1586.0 ± 10.2	34.579	2114.0 ± 12.0
34.695	288.23	H I	H18α					34.691	28.2 ± 8.7
34.940	286.20	CCH	$N = 12\text{–}11$			34.945	75.9 ± 6.0		
35.457	282.03	HCN	12–11	35.456	907.8 ± 8.7	35.457	521.7 ± 4.2		
35.632	280.65	HCN	$v_2 = 1; 12\text{–}11$f	35.639	237.6 ± 14.4	35.663	153.6 ± 4.8	35.669	31.8 ± 5.4
35.681	280.26	HCO$^+$	12–11						
36.268	275.73	HNC	12-11			36.266	144.0 ± 6.9		
36.604	273.19	o-H$_2$O	3_{12}-3_{03}	36.586	157.8 ± 15.6	36.601	276.0 ± 7.5		
36.737	272.20	^{13}CO	10–9	36.736	479.4 ± 18.0	36.737	166.8 ± 3.0	6.730	77.4 ± 4.2
37.137	269.27	p-H$_2$O	1_{11}–0_{00}	37.140	183.3 ± 6.9	37.138	257.1 ± 4.2	37.119	42.9 ± 11.7
37.416	267.27	H^{13}CN	13-12	37.425	258.9 ± 9.6	37.423	110.4 ± 6.6		
37.451	267.01	CN	$N = 10\text{–}9; v = 1$					37.448	21.6 ± 10.2
37.800	264.55	CN	$N = 10\text{–}9; v = 0$			37.799	171.6 ± 3.3		
37.845	264.24	CCH	$N = 13\text{–}12$					37.842	35.4 ± 11.1
38.076	262.63	^{12}CO	v=1;10-9	38.083	67.5 ± 72.3				
38.247	261.46	o-H$_2$O	7_{25}-8_{18}	38.235	16.5 ± 15.3				
38.408	260.36	HCN	13-12	38.421	4116.0 ± 23.4	38.424	2732.0 ± 20.1	38.416	2275.0 ± 10.8
+38.426	260.24	^{12}CO	10-9						
38.597	259.09	HCN	$v_2 = 1; 13\text{–}12$f	38.597	140.4 ± 24.9				
38.638	258.82	o-H$_2$O	6_{34}–5_{41}			38.638	131.1 ± 19.2		
+38.651	258.73	HCO$^+$	13–12						
38.791	257.79	o-H$_2$O	3_{21}-3_{12}			38.793	223.2 ± 6.3		
38.972	256.59	o-H$_2$O	8_{54}–7_{61}	38.969	250.2 ± 6.9	38.966	205.2 ± 6.9		
39.286	254.55	HNC	13–12	39.293	75.0 ± 5.7	39.279	139.5 ± 5.1		
40.282	248.25	p-H$_2$O	4_{22}-4_{13}	40.280	285.0 ± 3.9	40.278	113.1 ± 4.2		
+40.290	248.20	H^{13}CN	14–13						
40.406	247.49	^{13}CO	11–10	40.401	479.7 ± 4.2	40.402	185.7 ± 4.5	40.392	54.9 ± 4.2
40.517	246.81	p-H$_2$O	$v_2 = 1; 3_{12}$-3_{03}					40.510	5.7 ± 3.9
40.530	246.73	p-H$_2$O	$v_2 = 1; 8_{45}$-7_{52}	40.525	356.1 ± 3.6	40.524	220.2 ± 3.9		
40.750	245.40	CCH	$N = 14\text{–}13$			40.752	64.5 ± 4.2		
40.988	243.97	p-H$_2$O	2_{20}-2_{11}			40.992	102.0 ± 3.9	40.981	31.5 ± 4.5
+40.996	243.93	H I	H17α						
41.191	242.77	CN	$N = 11\text{–}10; v = 1$			41.201	21.3 ± 3.0		
41.358	241.79	HCN	14-13	41.356	876.0 ± 11.1	41.357	600.9 ± 3.9	41.358	16.5 ± 3.6
41.561	240.61	HCN	$v_2 = 1; 14\text{–}13$f	41.545	166.2 ± 11.4				
42.263	236.61	^{12}CO	11–10	42.263	3765.0 ± 24.0	42.265	2615.0 ± 13.2	42.253	2365.0 ± 12.6
43.162	231.68	H^{13}CN	15–14	43.156	114.6 ± 9.0				
43.655	229.07	CCH	$N = 15\text{–}14$					43.649	29.7 ± 3.0
44.073	226.90	^{13}CO	12–11	44.072	512.7 ± 10.5	44.078	262.8 ± 3.3	44.062	64.5 ± 3.0
44.308	225.69	HCN	15–14	44.303	852.3 ± 10.2	44.306	570.3 ± 5.4		
44.525	224.59	HCN	$v_2 = 1; 15\text{–}14$f	44.523	133.5 ± 22.8				
44.919	222.62	CN	$N = 12\text{–}11;v$=1	44.903	20.1 ± 9.3				
45.318	220.66	HNC	15–14	45.324	65.4 ± 7.5	45.323	160.5 ± 3.9		
46.098	216.93	^{12}CO	12–11	46.096	4356.0 ± 15.3	46.097	3009.0 ± 100.5	46.087	2370.0 ± 9.3
46.428	215.39	HN^{13}C	16-15	46.443	32.7 ± 16.2	46.439	20.4 ± 6.9		
46.922	213.12	p-H$_2$O	$v_2 = 1; 3_{21}$-3_{12}			46.918	7.5 ± 4.8		
47.053	212.53	o-H$_2$O	5_{23}–5_{14}			47.049	43.8 ± 6.6		
47.256	211.61	HCN	16-15	47.255	837.9 ± 9.9	47.255	570.0 ± 7.5		
47.487	210.58	HCN	$v_2 = 1;16\text{–}15$f			47.469	73.8 ± 12.6		
47.555	210.28	HCO$^+$	16–15			47.555	73.2 ± 11.7	47.565	28.2 ± 5.4
47.738	209.48	^{13}CO	13–12	47.737	488.1 ± 16.2	47.740	217.2 ± 1.8	47.726	80.4 ± 6.3
48.333	206.90	HNC	16-15			48.329	91.8 ± 1.5	48.337	20.7 ± 6.3
48.655	205.53	CN	$N = 13\text{–}12;v$=1			48.658	118.5 ± 3.6		
48.738	205.18	[N II]	2–1					48.725	73.5 ± 7.8
48.921	204.41	H I	H16α	48.924	212.4 ± 22.5	48.922	177.6 ± 3.3	48.918	102.3 ± 7.2
49.117	203.60	CN	$N = 13\text{–}12; v = 0$			49.121	219.9 ± 4.5		
49.932	200.27	^{12}CO	13–12	49.932	4329.0 ± 27.3	49.933	3387.0 ± 15.3	49.921	2252.0 ± 9.6
50.203	199.19	HCN	17–16	50.204	709.2 ± 22.5	50.205	552.3 ± 6.6		
50.521	197.94	HCO$^+$	17–16			50.515	117.6 ± 14.1		
51.402	194.55	^{13}CO	14–13	51.393	444.9 ± 22.5	51.381	298.5 ± 8.4		

Table 2. Unidentified strong lines in the spectrum of AFGL 2688.

$\bar{\nu}_0$ (cm^{-1})	λ_0 (μm)	$F(\times 10^{-18}\text{Wm}^{-2})$	Possible carriers
15.657	638.69	201.3 ± 9.0	NH$_2$
15.762	634.44	139.5 ± 8.7	H^{13}CN v2 ; ^{30}SiS
15.931	627.71	116.1 ± 8.4	SiO 11–10
16.547	604.34	193.8 ± 6.3	NH$_2$
16.675	599.70	122.7 ± 5.1	H^{13}CN v1+v2
16.856	593.26	304.8 ± 12.0	o-SH$_2$
16.998	588.30	193.8 ± 21.9	CH$_2$
17.927	557.82	194.1 ± 8.4	CH
18.766	532.88	122.1 ± 3.9	SiS ; SiO 13-12
18.945	527.84	195.0 ± 3.9	p-SH$_2$
19.440	514.40	159.9 ± 3.6	
20.122	496.97	130.5 ± 7.5	
21.208	471.52	201.6 ± 12.0	
29.287	341.45	141.9 ± 4.8	HCN v2+2v3 ; C$_{18}$O
31.479	317.67	134.7 ± 20.4	
31.778	314.68	114.9 ± 20.4	NH$_2$
32.665	306.14	150.3 ± 7.8	HCN $\nu_2 = 0$
36.432	274.48	109.5 ± 15.6	
38.842	257.45	105.9 ± 4.8	
39.685	251.98	100.5 ± 6.0	
47.456	210.72	101.7 ± 72.3	HCN $\nu_2 = 1$
47.522	210.43	128.1 ± 85.5	
49.589	201.66	146.1 ± 27.0	
50.814	196.80	114.9 ± 22.2	HCN 3v2

Table 3. Unidentified lines in the spectrum of AFGL 618.

$\bar{\nu}_0$ (cm^{-1})	λ_0 (μm)	$F(\times 10^{-18}\text{Wm}^{-2})$	Possible carriers
15.782	633.63	111.0 ± 18.9	H^{13}CN v2
16.472	607.09	129.3 ± 4.8	
18.461	541.68	206.7 ± 12.3	
19.444	514.30	116.1 ± 5.4	HCN maser?
19.579	510.75	110.7 ± 5.4	
27.396	365.02	150.3 ± 2.7	
29.715	336.53	189.6 ± 8.1	HCN 2v2
36.418	274.59	105.9 ± 28.8	

Table 4. Unidentified lines in the spectrum of NGC 7027.

$\bar{\nu}_0$ (cm^{-1})	λ_0 (μm)	$F(\times 10^{-18}\text{Wm}^{-2})$	Possible carriers
15.650	638.98	201.9 ± 9.0	NH$_2$
16.983	588.82	128.1 ± 20.1	CH$_2$
17.662	566.19	249.3 ± 30.6	NH$_2$
17.880	559.28	101.1 ± 10.8	CH
17.941	557.38	120.9 ± 13.2	H37ϵ
18.062	553.65	121.5 ± 5.1	H$^+$, He$^+$, C$^+$, S$^+$ 28β
18.939	528.01	181.8 ± 11.1	H34δ; p-SH$_2$
20.101	497.49	109.8 ± 16.2	H$^+$, He$^+$, C$^+$, S$^+$ 27β
48.138	207.74	100.5 ± 7.5	NH$_2$, H26ϵ